A GENERAL ANALYTIC APPROACH TO ANALYSING NONSTATIONARY STOCHASTIC PROCESSES IN THERMODYNAMIC SYSTEMS. PART III: PRACTICAL APPLICATION OF THE APPROACH

Igor Tkachenko[1*], Kostiantyn Tkachenko[2], Victoria Miroshnichenko[3], Boris Drenchev[4], Yuri Miroshnichenko[2] and Boris Yanachkov[1]

[1] *Institute of Metal Science, Equipment and Technologies with Hydro- and Aerodynamics Centre "Acad. A. Balevski", Bulgarian Academy of Sciences, 67 Shipchenski Prohod Blvd, 1574 Sofia, Bulgaria, e-mails: ift955@gmail.com; borisya0001@gmail.com*

[2] *Independent researcher, Ukraine, e-mail: konstantyn@gmail.com; miroviktoria105@gmail.com*

[3] *Metinvest Polytechnics, Metinvest Holding, Ukraine e-mail: miroviktoria105@gmail.com*

[4] *Institute of Electrochemistry and Energy Systems, Bulgarian Academy of Sciences, Acad. G. Bonchev St., Bl. 10, 1113 Sofia, Bulgaria, e-mail: b.drenchev@abv.bg*

Abstract. In continuation of the Part I and Part II of the article, where the analytic approach to studying a transient process evolution in a thermodynamic system was formulated and its basic features were considered, the final experimental verification stage of the approach development was elaborated, regarding the macroplastic deformation of single phase Face-Centered Cubic (FCC) polycrystals, as a typical case of the transient process provided by numerous experimental and specific theoretical data. Novel analytic expressions were derived to calculate the true stress–true strain curves for each of the modes of the plastic deformation. Based on the well experimentally grounded model for the development of "parallel–independent" processes in deformed metals, the true strain of a whole deformed crystal was determined under the conditions of monotonic tensile loading with a constant elongation rate.

[*] Corresponding author.

DOI: 10.7546/EngSci.LX.23.01.03

The strain limits for each deformation mode, resulting from the general definitions of the basic approach characteristics $s_j(t)$ and $n_j(t)$, were specified and related to the fracture strains for the corresponding crystal regions. Theoretical true stress–true strain curves predicted by the approach were compared with the experimental ones for polycrystalline Al, Ni, Cu and Ag. Over 97% accuracy is reached for the coincidence between experimental and calculated stress–strain curves, as well as of fracture strains in the considered metals. Some novel features of the dislocation mechanisms in Al, distinguishing it from the other investigated FCC metals, were theoretically revealed and shown to be in accordance with the known disembodied specific experimental data.

Keywords: macroplastic deformation, dislocation glide, analytic relations, true stress–true strain curves, FCC-polycrystals, different crystal deformation modes, dislocation mechanisms.

1. INTRODUCTION

As it was shown in Part I and Part II of the article, a transient process in a thermodynamic system may be well described using the analytic approach developed in [1–2]. The macroscopic plastic deformation of Face-Centered Cubic (FCC) single-phase polycrystals was considered as an example of a transient process, due to the most detailed relevant theoretical and experimental data available. The differences in the revealed modes of development of such a transient process were attributed to various types of dislocation barriers providing different resistances $\tilde{\sigma}_j$ to dislocation glide in the deformed crystal. This conclusion was confirmed by an evaluation of the dissociation stress for the dislocation barriers under the single and multiple slip conditions in Cu-single crystals. Due to the simultaneous presence of the dislocation barriers of the two revealed types in a deformed FCC crystal, the averaged dislocation glide resistance should be considered to analyse the stress–strain behaviour of the crystal as a whole. Besides, comparing such behaviour with the experimentally observed one provides important information about the practical applicability of the developed theoretical approach and the involved dislocation mechanisms.

So, aim of the article is to calculate the true stress–true strain diagrams for some FCC metals within the framework of the approach and compare the obtained results with the available experimental data.

2. THEORETICAL TRUE STRESS–TRUE STRAIN DEPENDENCIES

As it was shown in previous parts of the article, the parameter $s(\sigma, t) \equiv (\tilde{\sigma}/\sigma)^n$ provides the integrated characteristic of the state of a loaded crystal with respect to its macroplastic flow under the two conditions $\sigma = \text{const}$ and $\sigma = \sigma(t)$. The most important practical case of a monotonous tensile loading at a constant elongation rate will be considered below. In order to obtain expressions describing time evolution of an applied true stress σ for the two deformation modes on the basis of the dependencies $s_j = s_j(t)$, some basic properties of the relevant quantities must be taken into account. Namely, $n_j(t) > 0$, $d\sigma/dt > 0$ according to the early given definitions. Besides, it follows from relations (14) and (15) of the paper [1] that $ds_j(t)/dt = 0$ at $t = \hat{t}_j$. Let us consider further the quantities $z_j \equiv \ln(1/s_j)$ as functions of two variables $x_j \equiv n_j$, $y_j \equiv \ln(\sigma/\overleftarrow{\sigma}_j)$, $z_j(x, y) = x_j \cdot y_j$, where $x_j = x_j(t)$, $y_j = y_j(t)$, $z_j = z_j(t)$. For the extreme points of the functions $z_j = z_j(t)$ reached by the times $t = \hat{t}_j$, one can write $\partial z_j(a, b)/\partial x = 0$, $\partial z_j(a, b)/\partial y = 0$, where $x(\hat{t}_j) = a_j$, $y(\hat{t}_j) = b_j$. On the other hand, one has to obtain $\partial z_j/\partial x \approx y_j$, $\partial z_j/\partial y \approx x_j$ under the conditions $x_j(t) \gg a_j$ and $|y_j(t)| \gg b_j$. Therefore, in general case, it may be written $\partial z_j/\partial x = y_j - b_j$, $\partial z_j/\partial y = x_j - a_j$. Introducing the marks $p_j \equiv \partial z_j/\partial x$ and $q_j \equiv \partial z_j/\partial y$, one arrives at a partial differential equation describing the dependencies $y_j = y_j(x_j)$ under the just given conditions:

$$(p_j + b_j) \cdot (q_j + a_j) - z_j = 0.$$

Assuming for simplicity that the two quantities x_j and y_j begin to evolve simultaneously with time, one arrives at relations as solutions of the above differential equation in partial derivatives:

$$y_j = \text{sgn}(y_j) \cdot (-x_j + C_j), \tag{1}$$

where $\text{sgn}(y_j) = 1$ if $y_j > 0$ and $\text{sgn}(y_j) = -1$ if $y_j < 0, C_j = 2a_j = 2b_j$. As it follows from equation (1), the form of the time dependence $\sigma = \sigma(t)$ for a deformation mode depends on a sign of the variable $y_j \equiv \ln(\sigma/\overleftarrow{\sigma}_j)$, i.e., a value of the ratio $\sigma/\overleftarrow{\sigma}_j$ as compared to unity. As it was inferred in [1–2], the first mode of the macroplastic deformation develops by the single dislocation glide, whereas the second deformation mode is controlled by the multiple slip. On the other hand, it was also shown that the dislocation barriers formed under the single slip conditions are able to dissociate at low applied stresses, in contrast to the insurmountable dislocation barriers appearing in the course of the multiple glide of dislocations. Thus, based on these results for the first

deformation mode it can be written $\sigma > \overleftarrow{\sigma}_1$, i.e., $s_1 < 1,\ y_1 > 0$, and then using equation (1) and relation (14) from [1] it is found:

$$\sigma(t) = \overleftarrow{\sigma}_1 \exp\left[-n_1(t) + C_1\right]; \quad n_1 = \frac{C_1 \pm \sqrt{C_1 + 4\ln s_1(t)}}{2}, \tag{2}$$

where $C_1 = 2\sqrt{\ln\left[1/\ln(A_1/2)\right]}$.

For the case of the second mode of the crystal deformation it can be written $\sigma < \tilde{\sigma}_2$, i.e., $s_2 > 1,\ y_2 < 0$, and from equation (1) and relation (15) from [1] it is obtained:

$$\sigma(t) = \overleftarrow{\sigma}_2 \exp\left[n_2(t) - C_2\right]; \quad n_2 = \frac{C_2 \pm \sqrt{C_1 - 4\ln s_2(t)}}{2}, \tag{3}$$

where $C_2 = 2\sqrt{\ln\left[1/\ln(A_2/2)\right]}$.

Based on the definitions of the constants C_j, one finds $2 < A_1 < 2e$; $A_2 > 2e$. Since the crystal deformation under the monotonous loading conditions is considered in the paper, the upper signs in the formulae for $n_j(t)$ have to be used within the time intervals $t < \hat{t}_j$, whereas the bottom signs correspond to the intervals $t > \hat{t}_j$. According to the definitions of the quantities s and n, the following conditions $s_j > 0$ and $n_j > 0$ have to be also fulfilled. Using expressions (14), (15) from [1] for $s_j = s_j(t)$ and (2), (3) for $n_j = n_j(t)$, it is easy to show that joint satisfaction of these conditions is possible, i.e. the dependencies $\sigma_j = \sigma_j(t)$ are valid only within the time intervals $0 < t < \hat{t}_1(1 + \sqrt{[2 - (A_1/e)]})$ and $0 < t < \hat{t}_2(1 + \sqrt{A_2 - 2})$ for the first and second deformation mode, respectively. An adequate description of the input time dependencies $s_j = s_j(t)$ is also provided by the just obtained relations (2), (3) within the time intervals. Under the condition of tensile loading at constant deformation rate $\dot{\varepsilon}$, one can proceed to the new independent variable $\varepsilon = \dot{\varepsilon} \cdot t$ instead of t in formulae (2) and (3), and then the true stress–true strain curves can be obtained using the quantity $\varphi = \ln(\varepsilon{+}1)$. The characteristic theoretical dependencies $\sigma_j = \sigma_j(\varphi)$ illustrating the modelling potential of equations (2) and (3) for the revealed deformation modes are shown in Fig. 1, where a close coincidence of the calculated dependencies with the ones corresponding to the single and multiple dislocation glide, respectively, can be seen.

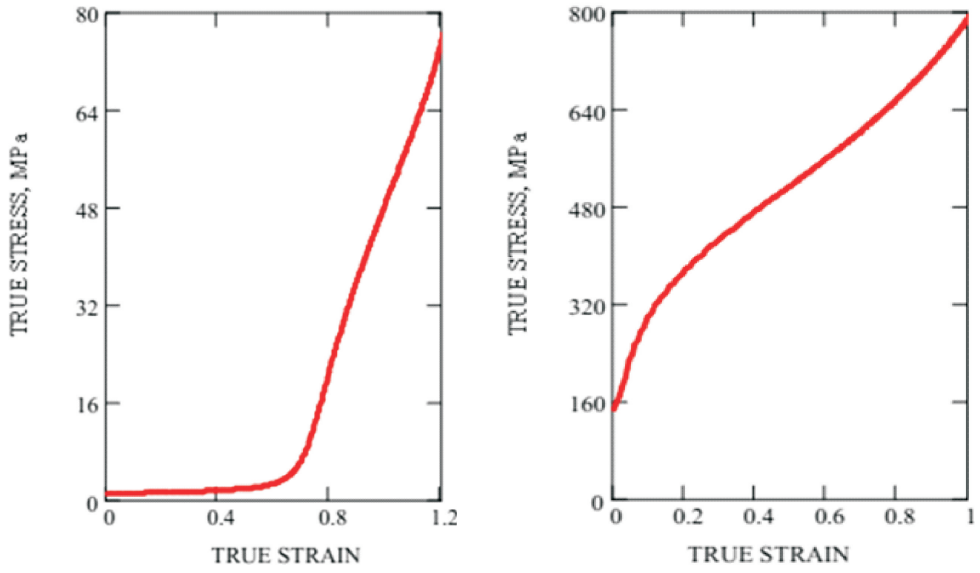

Fig. 1. Calculated characteristic true stress–true strain curves for the revealed modes of the macroplastic deformation: (a) first mode; (b) second mode

3. COMPARISON WITH EXPERIMENT: RESULTS AND DISCUSSION

As it follows from the obtained theoretical results, the developed approach allows to predict the stress–strain behaviour of a FCC crystal based on the data related to the mechanisms of dislocation motion and vice-versa, namely to describe the regularities of dislocation glide based on the macroscopic tensile behaviour of a loaded crystal. Unfortunately, in the case the necessary quantitative data related to the stress and time dependencies of the dislocation glide parameters are usually very limited and not available for most polycrystalline metals in particular. Therefore, the tensile stress–strain curves for polycrystalline Ag, Cu, Ni and Al will be analysed to reveal some features of their respective dislocation glide mechanisms [3].

It is obvious that the most detailed description of the stress–strain behaviour within the framework of the presented approach is possible only by taking into account the predicted joint development of the two revealed modes of the plastic flow in a deformed FCC crystal [1–2]. As follows from the definition of the dislocation and crystal state parameter $s(\sigma, t) \equiv (\tilde{\sigma}/\sigma)^n$, the two deformation modes develop under the action of the same stress equal to

the applied one σ. However, the modes result in different time dependencies of the parameter s, $s_j = s_j(t)$, as well as the true strain values at a given acting stress σ, as seen from the above equations (2) and (3). That is why the joint development of the two deformation modes in real crystals was described according to the model considering a combination of "parallel–independent" processes [4]:

$$\varphi = V_1\varphi_1 + (1 - V_1)\varphi_2, \tag{4}$$

where φ is a global true strain of a crystal; φ_1 is a true strain of crystal regions where the first deformation mode develops; V_1 is a volume fraction of the just mentioned regions; φ_2 is a true strain of crystal regions where the second deformation mode develops. Besides, the application of this technique is confirmed by the experimental data for FCC metals well described within the framework of the above model [4]. A graphic illustration of the used technique is shown in Fig. 2 by the following dependencies true stress–true strain: (i) the dependence describing the deformation of crystal regions where the first mode of the plastic flow develops, curve 1; (ii) the dependence relating to the deformation of crystal regions where the second mode develops, curve 2; (iii) the dependence corresponding to the deformation of a whole crystal, curve 3. The considered curves were calculated taking into account the above results according to which the first and the second deformation modes are limited in time by the points:

$$t_1^{\lim} = \hat{t}_1(1 + \sqrt{[2 - (A_1/e)]}), \quad t_2^{\lim} = \hat{t}_2(1 + \sqrt{A_2 - 2}),$$

respectively. The levels of acting stress, corresponding to the time limits $t_1^{\lim}$ and $t_2^{\lim}$, are also shown in Fig. 2 as curves 4 $\left(\sigma_1^f\right)$ and 5 $\left(\sigma_2^f \equiv \tilde{\sigma}_2\right)$, respectively. According to the above definitions of the quantities $t_1^{\lim}$ and $t_2^{\lim}$, the stresses σ_1^f and $\sigma_2^f \equiv \tilde{\sigma}_2$ are considered to initiate the fracture of crystal regions where the first and second deformation modes develop, respectively.

Based on this, the global true strain levels of the crystals φ_1^f, φ_2^f can be defined, reaching which initiates fracture (crack nucleation) in the corresponding crystal regions, Fig. 2.

Using now formulae (2) and (3) in order to calculate φ_j for each of the deformation modes at various levels of the same acting stress σ, together with the general relation (4) and a fitting procedure, the values of the model constants $\widehat{t}_j$, A_j, $\tilde{\sigma}_j$, as well as the volume fraction V_1, can be obtained, making the most adequate theoretical description of the experimental stress–strain dependencies possible. The values of the above parameters, providing more than 97% accuracy in fitting the theoretical and experimental true tensile curves

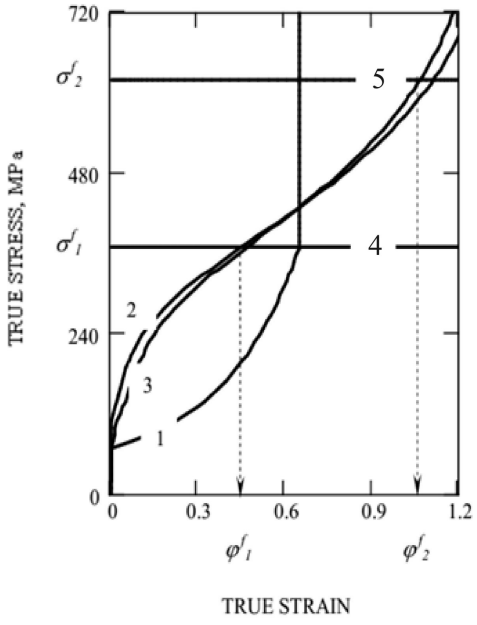

Fig. 2. Typical illustrative graphic relations of the true stress–true strain dependencies, corresponding to each deformation mode, curves 1 and 2, lines 4 and 5; the whole crystal deformation, curve 3

over the whole range of measured deformations for polycrystalline metals, are given in Table 1, [3]. Additionally, for the deformation modes starting stresses $\sigma_j(0)$ are also given for each metal there. These stresses provide the onset of the deformation modes and were calculated using equations (2) and (3) at $t = 0$. There are also the calculated fracture strains φ_j^f, as well as the experimental values of the strain-to-fracture φ_{exp}^f for each metal in Table 1, [3]. The predicted and experimental true stress–true strain dependencies together with the corresponding fracture stresses are plotted in Fig. 3.

As can be seen in Table 1, only the model parameter $\widehat{t}_1$ demonstrates well-defined changes with the stacking fault energy. One of the consequences of the changes is the decrease of φ_1^f with the growth of the energy, i.e., during the transition from Ag to Al. This result is in agreement with the experimental data showing an increase in the plasticity of FCC metals and alloys with a decrease in the stacking fault energy [5]. It is also seen that the experimental fracture strains φ_{exp}^f are close to the corresponding calculated ones φ_1^f for Al, Ni, Cu and φ_2^f for Ag. The lower levels of the experimental fracture strains in comparison with the corresponding theoretical ones may be explained by inevitable presence of the structural defects facilitating the fracture of real crystals.

Table 1. The approach parameters providing 97% fitting the calculated and experimental true stress–true strain tensile curves for some FCC polycrystalline metals

Metal	A_1	$\hat{t}_1$ (s)	$\widetilde{\sigma}_1$ (MPa)	$\sigma_1(0)$ (MPa)	φ_1^f	V_1	A_2	$\hat{t}_2$ (s)	$\widetilde{\sigma}_2$ (MPa)	$\sigma_2(0)$ (MPa)	φ_2^f	φ_{exp}^f
Al	5.43	35	50	24.6	0.21	0.60	$10^{5.6}$	32	125	21.4	1.90	0.18
Ni	2.80	240	95	94.0	0.38	0.10	$10^{3.6}$	13	860	164.0	0.45	0.33
Cu	3.50	450	80	70.0	0.46	0.10	$10^{4.4}$	19	618	112.0	1.06	0.40
Ag	2.20	550	75	81.0	0.75	0.05	$10^{4.0}$	10	365	68.00	0.52	0.42

The data given in Table 1 show particularly that the macroplastic flow in polycrystalline Al develops mainly by the dislocation mechanism ($V_1 = 60\%$) associated with the first deformation mode, i.e., by the single dislocation glide. It follows also from the relation of the starting stresses $\sigma_j(0)$ of the modes $\sigma_1(0) > \sigma_2(0)$ that the single slip in Al begins after the onset of the multiple one associated with the second deformation mode, i.e., after formation of a developed dislocation cell structure. On the other hand, it can be seen in Fig. 3

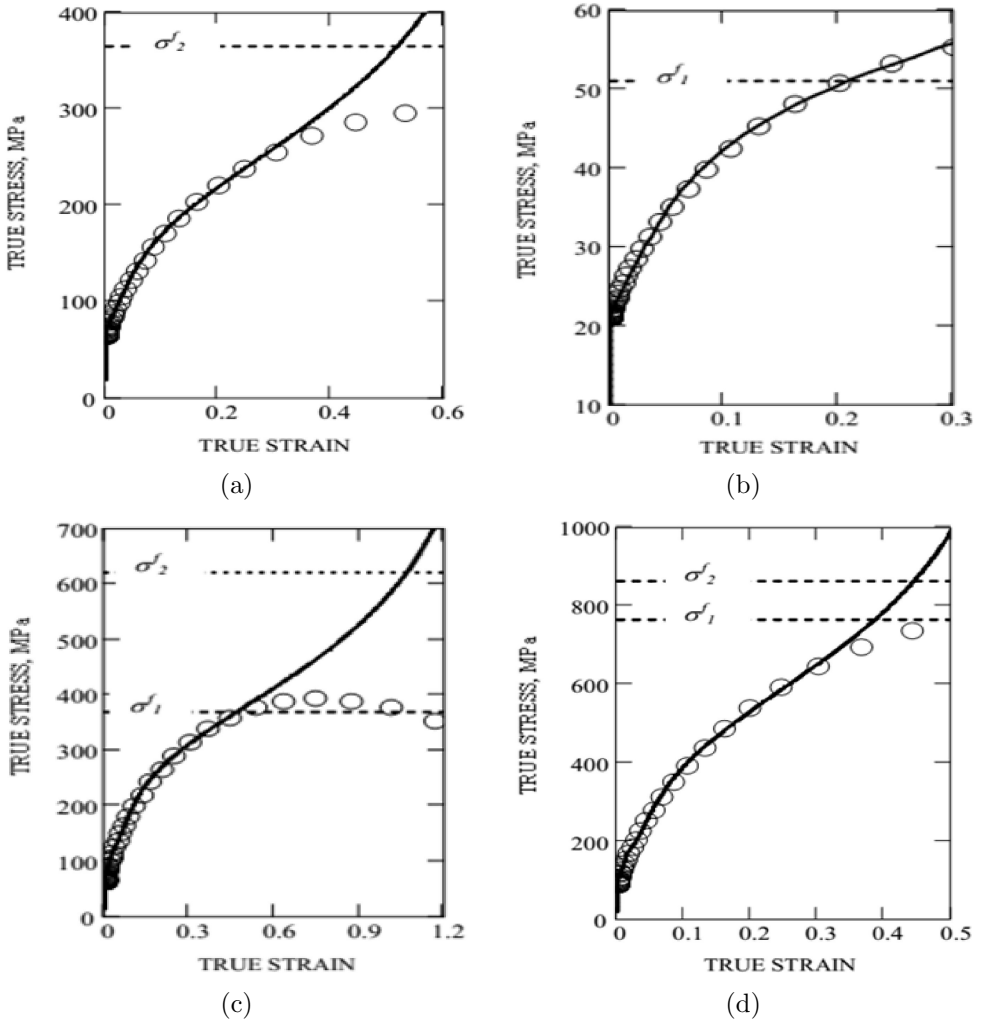

Fig. 3. Calculated (lines) and experimental (circles) true stress–true strain dependences for some FCC polycrystals: (a) Ag; (b) Al; (c) Cu; (d) Ni

and Table 1 that $\sigma_1^f \approx \tilde{\sigma}_1$. It implies that the single dislocation glide in Al is practically limited by the stage of the micro-deformation, since the thermally activated dissociation of stable dislocation barriers is only possible at $\sigma \geq \tilde{\sigma}_1$, which immediately leads to the fracture of the corresponding crystal regions $\tilde{\sigma}_1 \approx \sigma_1^f$. This in turn means that only insurmountable dislocation barriers are formed during the deformation of an aluminium polycrystal. Thus, it can be concluded that the single slip in polycrystalline Al develops probably within dislocation cells that reach a favourable orientation in the course of multiple slip: the walls of the cells are composed of dislocation bonds that cannot be overcome by gliding dislocations, as shown earlier. This conclusion is consistent with numerous experimental data related to the deformation of pure Al, solid oriented single- and polycrystals. Particularly, the following is observed, namely: (i) single slip, possibly under creep conditions [6]; (ii) weak dependence of the flow stress on the grain size at different strains [7]; (iii) strong dependence of stresses on the size of the dislocation cell [8]; (iv) alternation of dislocation cells, in which the multiple slip traces are observed ($\sim$50%) with the cells without the traces [9–10]; (v) impenetrability of the cell walls to gliding dislocations [6, 8]; (vi) absence of the intergranular fracture mode under any loading conditions [11].

In contrast to Al, in such FCC metals as Ni and Cu, the second deformation mode associated with the multiple dislocation glide has the largest ($1 - V_1 = 90\%$) contribution to the global crystal deformation. At that, the first deformation mode, corresponding to the single slip, starts before the onset of the multiple one $\sigma_1(0) < \sigma_2(0)$, and develops in combination with the formation and further dissociation of the surmountable dislocation barriers, as follows from the relation $\tilde{\sigma}_1 \ll \sigma_1^f$. As a result, a considerable strain is required to reach the ultimate strain hardening, i.e. the fracture of crystal regions where the first deformation mode develops in such polycrystals compared to Al (See Table 1). Based on the above, it can be concluded that the macroplastic deformation of Ni and Cu polycrystals starts with the single slip within some favorably oriented grains (10%) or grain boundaries. Particularly, the gliding dislocation segments within such grains are able to reach the grain boundaries where insurmountable dislocation barriers can be formed contrary to the grain interiors. These conclusions coincide with the experimental data showing: (i) the relatively strong dependence of the flow stress on grain size for Cu [12]; (ii) dislocation glide in interiors of only 10% of grains in Cu at the beginning of the plastic flow [13]; (iii) development of the intergranular fracture under the certain loading conditions in Cu, Ni and Ag [11].

Additional qualitative information about the features of the dislocation mechanisms in the considered metals can be obtained in particular by comparing the values of the parameter $\hat{t}_2$ given in Table 1 for the metals. As can be seen, Al is characterized by the considerably higher $\hat{t}_2$ value than the other metals. As a result, the same value of the probability $P_{II\,2}(t)$, characterizing the state of crystal regions where the second deformation mode develops, is reached in Al at a higher strain than that in the other metals [1–2]. It suggests in particular that a higher level of deformation is required for Al to obtain the same dislocation cell structure as in Ni, Cu and Ag. This conclusion is confirmed by the results of direct measurements of cell sizes in Al and Cu at comparable strain intervals [14–16].

4. CONCLUSIONS

1. In continuation of the Part I and Part II of the article, where the analytic approach to studying a transient process evolution in a thermodynamic system was formulated and its basic features were considered, the final experimental verification stage of the approach development was elaborated with respect to the macroplastic deformation of single phase polycrystals, as a typical case of a transient process provided by numerous experimental and specific theoretical data.
2. Proceeding from the approach basic relations, novel analytic expressions were derived to calculate the true stress–true strain curves for each of the modes of the plastic deformation development. Further, based on a well experimentally substantiated model of the development of "parallel–independent" processes in deformed metals, true strain of whole deformed crystals was determined under the conditions of monotonic tensile loading with a constant elongation rate.
3. The strain limits for each deformation mode resulting from the general definitions of the basic approach parameters $s_j(t)$ and $n_j(t)$ were specified and associated with the fracture strains for the corresponding crystal regions.
4. The theoretical true stress–true strain curves predicted by the approach were compared with the experimental ones for polycrystalline Al, Ni, Cu and Ag. For the considered metals, over 97% accuracy is reached for the experimental and calculated stress–strain curves and for the fracture strains.
5. Some novel features of the dislocation mechanisms in Al, distinguishing it from the other investigated FCC metals, were revealed and shown to be in agreement with the known disembodied specific experimental data.

ACKNOWLEDGEMENTS

This article was partially supported by the European Regional Development Fund within the OP "Science and Education for Smart Growth 2014– 2020", Project CoE "National center of mechatronics and clean technologies", No BG05M2OP001-1.001-0008-C08. Another support is obtained by Bulgarian National Science Found within the project КП-06-Н27/19 "Study on HELP Mechanism of Hydrogen Embrittlement by Application of Advanced Powerful Hybrid Computer Architectures: Model Simulations and their Experimental Verification". The authors would like to express their gratitude to Prof. Tony Spasov and Dr. Veselina Rangelova for their valuable discussions and analysis.

REFERENCES

[1] I. Tkachenko, V. Miroshnichenko, B. Drenchev, B. Yanachkov, and M. Kolev, A General Analytic Approach to Analysing Nonstationary Stochastic Processes in Thermodynamic Systems. Part I: Formulation of the Approach, *Engineering Sciences* (2022) **LIX** (3) 48–64.

[2] I. Tkachenko, K. Tkachenko, Y. Miroshnichenko, B. Drenchev, and B. Yanachkov, A General Analytic Approach to Analysing Nonstationary Stochastic Processes in Thermodynamic Systems. Part II: Basic Features of the Constitutive Equation Analytic Solutions, *Engineering Sciences* (2022) **LIX** (4) 41–56.

[3] I. Kovacs and G. Voros, *International Journal of Plasticity* (1996) **12** 35–37.

[4] B. Faucher, A. Krausz, *Z. Naturforsch.* (1980) 35a 1152–1161

[5] M. Kassner, *Fundamentals of Creep in Metals and Alloys*, Butterworth-Heinemann, Berlin (2015).

[6] R. Honeycombe, *The Plastic Deformation of Metals*, Edward Arnold, London (1984).

[7] I. Kovács, N. Chinh, and E. Kovács-Csetényi, *Physica Status Solidi* (A) (2002) **194** 3–18.

[8] R. Maass and P. Derlet, *Acta Materialia* (2018) **143** 338–363.

[9] T. Tabata, H. Fujita, M. Hiraoka, and S. Miyake, *Philosophical Magazine A* (1982) **46** 801–816.

[10] T. Malis and K. Tengri, *Acta Metallurgica (*1979) **41** 25–32.

[11] M. Ashby, C. Gandhi, and D. Taplin, *Fracture-mechanism Maps and Their Construction for FCC Metals and Alloys. Overview*, Pergamon (1983) **3**.

[12] H. Conrad, *Metallurgical and Materials Transactions A* (2004) **35** 2681–2695.

[13] J. Huang, Y. Zhu, H. JIANG, and T. Lowe, *Acta Materialia* (2001) **49l** 1497–1505.

[14] T. Tabata, S. Yamanaka, and H. Fujita, *Acta Metallurgica* (1978) **26** 405–411.

[15] P. Landau, R. Shneck1, G. Makov, and A. Venkert, *Journal of Physics: Conference Series 241* (2010).

[16] D. Knoesen and S. Kritzinger, *Acta Metallurgica* (1982) **30** 1219–1222.

Received August 29, 2022